Femoral bone structure and mechanics at the edge and core of an expanding population of an invasive frog, *Xenopus laevis*

Maïtena Dumont[1,2,*], Anthony Herrel[3,4,5,6], Julien Courant[3], Pablo Padilla[3,7], Ron Shahar[1], Joshua Milgram[1]

[1]Laboratory of Bone Biomechanics, Koret School of Veterinary Medicine, The Robert H. Smith Faculty of Agriculture, Food and Environment, PO Box 12, 7610001, Rehovot, Israel.
[2]Max-Planck-Institute for Sustainable Materials, MPISM, D-40237, Düsseldorf, Germany
[3]UMR 7179 C.N.R.S/M.N.H.N., Département Adaptations du Vivant, Bâtiment d'Anatomie Comparée, 55 rue Buffon, 75005, Paris, France.
[4]Department of Biology, Evolutionary Morphology of Vertebrates, Ghent University, Ghent 9000, Belgium.
[5]Department of Biology, University of Antwerp, Wilrijk 2610, Belgium.
[6]Naturhistorisches Museum Bern, 3005 Bern, Switzerland.
[7]Laboratory of Ecology and Conservation of Amphibians (LECA), Freshwater and Oceanic science Unit of reSearch (FOCUS), University of Liège, Liège, Belgium

Corresponding author: Maitena Dumont maitena.dumont@gmail.com

Abstract

Understanding how living tissues respond to changes in their mechanical environment is a key question in evolutionary biology. Invasive species provide an ideal model for this as they are often transplanted between environments that differ drastically in their ecological and environmental context. Spatial sorting, the name given to the phenomenon driving differences between individuals at the core and edge of an expanding range, has been demonstrated to impact the morphology and physiology of *Xenopus laevis* from the invasive French population. Here, we combined a structural analysis using micro-CT scanning and a functional analysis by testing the mechanical properties of the femur to test whether the increased dispersal at the range edge drives differences in bone morphology and function. Our results show significant differences in the inner structure of the femur as well as bone material properties, with frogs from

Journal of Experimental Biology • Accepted manuscript

the centre of the range having more robust and resistant bones. This is suggestive of an energy allocation trade-off between locomotion and investment in bone formation or alternatively may point to selection for fast locomotion at the range edge. Overall, our results further provide insights on the growth of the long bones and the formation of trabecular bone in frogs.

Keywords: *Xenopus laevis*, femora, bone cortical analysis, biomechanical properties, invasive species.

Introduction

Invasive species are among the principal causes of the current loss of biodiversity worldwide (Mollot et al., 2017; Simberloff et al., 2013). However, invasive species also inadvertently provide an exceptional model to study and understand the evolutionary mechanisms underlying range expansion (Burton et al., 2010; Tingley et al., 2014) and the mechanisms driving the evolution of dispersal phenotypes (Philips et al., 2006; Shine et al., 2011). The African clawed frog, *Xenopus laevis,* a predominantly aquatic frog from Sub-Saharan Africa, has become invasive on a global scale (Tinsley et al., 2009; Measey et al., 2012) and was introduced into France in the early 1980s (Fouquet, 2001). Since its introduction the species has spread rapidly, and is now present in at least five provinces in France (Vimercati et al., 2019). Although primarily aquatic, animals also disperse overland during heavy rainfall (Courant et al., 2019a).

Previous studies have demonstrated significant differences in the morphology and physiology in frogs from the core and edge of the range in the French population, a finding attributed to spatial sorting (Courant et al., 2017, 2019a; Louppe et al., 2017, Padilla et al., 2019, 2020). Spatial sorting is a consequence of rapid population expansion resulting in individuals with a different phenotype being present at the edge of the range. This subsequently results in non-random mating with other individuals that exhibit a similar dispersal phenotype (i.e. only animals that are good dispersers

will encounter each other at the edge of the invasive range and will thus mate; see Burton et al., 2010; Shine et al., 2011; Chuang and Peterson, 2016). Individuals at the edge of the range of the invasive population of *X. laevis* in France show a higher *in vivo* endurance capacity (Louppe et al., 2017), a lower standard metabolic rate (SMR, Louppe et al., 2018), and a lower investment in reproduction (Courant et al., 2017) when compared to individuals from the core of the range. In addition, *X. laevis* from the edge of the range have longer legs and stronger hind limb muscles with a greater physiological cross-sectional area (Louppe et al., 2017; Padilla et al. 2019). These differences at least partly account for the greater dispersal rates and dispersal distances observed for individuals at the range edge (Courant et al., 2019a).

In addition, sexual dimorphism has been observed in *X. laevis* (Louppe et al., 2017; Padilla et al., 2019). For example, despite their smaller size compared to females, male *X. laevis* have relatively larger and more powerful muscles (Padilla et al. 2019), relatively longer legs, and greater stamina than females (Louppe et al., 2017). These differences have been suggested to be responsible for the greater dispersal observed in males compared to females (Courant et al., 2019a).

Bone is a living tissue that responds to the external forces exerted upon it by modeling (e.g. Currey, 2002, Kular et al., 2012; Stoltz et al., 2018). Given the known sexual dimorphism, and differences in morphology, physiology, and endurance in individuals from the edge and core of the range, we predicted differences in bone structure and mechanical properties between these individuals. Specifically, we predicted that individuals from the edge would show long bone adaptations consistent with the increased frequency and higher loads to which they are subjected during locomotion, and that these differences would be more pronounced in males. Alternatively, the energy allocated to locomotion and muscle development may impact the energy available to bone growth resulting in the opposite pattern. To test these hypotheses, we focused on the femur as the extensor muscles attached to it are the primary source of the power needed during jumping (Prikryl et al., 2009; Padilla et al., 2019). We tested for differences in cortical thickness, mean cross-sectional area of the bone, its second moment of area, bone mineral density, Young's modulus, and the bending yield stress and strain between individuals from the core and the edge of the range as well as between males and females.

Material and methods

The samples used in this study were harvested from individuals collected by Courant et al. (2019a). Animals were collected and euthanized under permit from the Préfet des Deux-Sèvres. Euthanasia was performed by injection of a lethal dose of sodium pentobarbital. The study sites were located in the expanding range of *X. laevis* in Western France (Courant et al. 2019a). The edge and core sites were defined as in Courant et al. (2019a) and Padilla et al. (2019). Frogs were captured in 18 ponds from May to October 2014 and during spring 2016. The left femora were dissected free of soft tissues and stored in ethanol (70% solution). In total, 36 samples were investigated (8 females and 10 males collected from core sites; 9 females and 9 males collected from the edge sites). The age of the individuals ranged from < 1 year to 6 years (Courant et al. 2019b). Despite differences in core and edge populations (e.g. in endurance capacity, metabolic rate, and muscles cross-section areas), no differences in growth rate are present (Courant et al. 2019b). Consequently, we here use femur length as a proxy for the age and size of the animals.

Micro- CT scanning

All bones were scanned using a desktop Micro- CT scanner (Skyscan® 1174, micro-CT scanner, Skyscan, Belgium). Each bone was placed in a plastic tube and stabilized in agar. The X-ray source was set at 50 kVp and 800 µA. All specimens were scanned over 180º with a rotation step of 0.4 degrees and exposure time of four seconds. A 0.25 mm aluminium filter was used to decrease beam hardening effects. The entire femur was scanned at an isotropic pixel spacing of 33.6 µm. The diaphysis of one of the samples was scanned at higher resolution (9.6 µm) and compared with the same femur scanned at lower resolution to ensure the quality and reliability of the cortical diaphysis measurements of the scan at lower resolution. Epiphyses were scanned at an isotropic pixel spacing between 7.5 µm to 12.2 µm (depending on the size of the femur).

Scans were reconstructed and analyzed using commercial software (NRecon® version 1.6.9.18, Bruker®, Kontich, Belgium and CT analyzer®, Bruker®, Kontich, Belgium, respectively). A region of interest (ROI) of 150 slices, centered on the mid-diaphysis, was used for the cortical analysis. The mid-diaphysis is chosen by convention and according to previous research showing that this is the location where peak strains are highest (e.g. Biewener and Taylor 1986). The trabecular analysis was carried out on the distal and proximal epiphyses. Regions of interest of 250 slices starting at the wedge-shaped margin of the periosteal bone (as described by Rozenblut and Ogielska 2005) were used. Two phantoms with known density (0.25 g/cm^3 and 0.75 g/cm^3) were scanned using the identical parameters used for scanning the femora allowing the calculation of the bone mineral density (BMD) of the cortical diaphysis. Morphometric analysis and BMD evaluation was carried out using dedicated software (Skyscan® CT Analyser, version 1.15.4, Skyscan, Belgium). Three dimensional representations of the various bones were obtained using Amira (FEI, version 5.6.0, Hillsboro, Oregon, USA).

Bone characterization

The results of the cortical analysis for all femora are listed in Table 1, using the abbreviation and terminology of Bouxsein et al. (2010). The results of the cortical analysis included the total cross-sectional issue area (T.Ar, in mm^2), the cortical bone area (B.Ar, in mm^2), the average cortical thickness (Cs.Th, in mm), the average second moment of area Imin and Imax (Av.MMI(max) and Av.MMI(min), in mm^4), the mean polar moment of area (MMI(polar), in mm^4) and the mean eccentricity (Ecc). For the trabecular analyses only a subset of individuals was used (see supplementary table 1 and supplementary Table 4) and only the distal epiphysis was used as proximal epiphyses often had few trabeculae. The variables extracted for the trabecular analysis included bone volume (BV, in mm^3), tissue volume (TV, in mm^3) bone volume fraction (BV/TV, in %), trabecular number (Tb.N, in mm^{-1}), trabecular thickness (Tb.Th, in mm), trabecular separation (Tb.Sp, in mm).

Three-point bending

Three-bending mechanical testing was conducted not only for comparative purposes as the largest and most comprehensive dataset on mechanical properties of long bones was obtained by this method (Erickson et al. 2002), but bending is also the primary loading direction and source of bone strain in limb bones of tetrapods (e.g. Biewener and Taylor 1986). Moreover, Currey demonstrated that bones tend to fail on the tensile side during bending (Currey, 2002).

Three-point bending was performed on six femora from each group using a custom-built micro-mechanical testing device. The caudal aspect of the diaphysis of each bone was positioned on the supports of the stationary anvil such that the support of the moving anvil contacted the bone at its midpoint. The distance between the stationary supports was 15 mm (note that we did not adjust the span based on femur length which may have induced some bias in our results). A preload of 1.5 to 1.8 N was applied to the sample prior to testing. Each specimen was tested under displacement control and at a rate of 300 µm/min to fracture which was characterized by a sudden decrease in load. The loading rate was lower than in previous studies as these are predominantly aquatic frogs for which loading rates can be assumed to be lower. Yet, this remains hypothetical as no *in vivo* loading rates have been measured or estimated for this species. The force-displacement data obtained were then converted to stress and strain using beam theory where:

$$\text{Stress } \sigma = F \times \frac{L \times D}{8 \times I}$$

Where F is the load applied (N), L the span used in the bending test (mm), D the diameter at the midpoint of the femur (mm) and I the inner second moment of area (mm^4). The diameter at the midpoint of the femur (D) was the average cortical diameter determined from ten different CT images

$$\text{Strain } \varepsilon = \Delta \times \frac{6 \times D}{L^2}$$

Where Δ is the displacement (mm), D the diameter of the bone (mm), and L the span of the stationary anvil (mm).

The Young's modulus (N/mm^2 or MPa) of the bone was obtained from the slope of the linear part of the stress-strain curve. In addition, the stress and strain at the yield

point and the point of fracture were also determined. The yield point was determined as the point which marked the transition between the linear part and the plastic area of the stress-strain curve (e.g., Turner 2006; Sharir et al. 2008): it was determined by successive steps on the curve by obtaining linear regression. At this yield point, the yield stress (σ_y) and yield strain (ε_y) are determined. Fracture stress and strain represents the point where the bone breaks. The bones were stored in ethanol since the samples were harvested in 2004 and 2006. Whereas prior work suggested that mechanical properties of bones stored in ethanol for less than 14 days and up to 100 days (e.g. respectively Turner and Burr, 1993; Linde and Sorensen, 1993) are not affected, this does not seem the case for long storage as in our case. Vesper et al. (2017), did indeed notice an increase in bone stiffness and elastic modulus after long storage (~7 weeks) in ethanol. Consequently, we may overestimate stiffness and elastic modulus. However, since all bones were subjected to the same condition results should be consistent and comparable between different groups (core versus edge).

Statistical analysis

All data were Log_{10}-transformed before analyses to ensure normality and homoscedasticity of the data using Shapiro Wilk's and Levene's tests (see supplementary tables 2 and 3). All variables were normally distributed and all showed homogeneity of variances except Yield stress (supplementary table 3).

First, we ran a univariate analysis of covariance (ANCOVA) with femur length as a covariate to test for differences in bone mineral density between populations and sexes. We also tested interaction between population and sex. Next, we ran multivariate analyses of covariance (MANCOVA) with femur length as a covariate on three different data sets: 1) cortical bone parameters, 2) trabecular measures of the distal epiphysis, and 3) the biomechanical measurements (Young's modulus, stress at/to fracture, yield stress and yield strain). Subsequently we ran univariate ANCOVAs with sequential Bonferroni correction to test which variables differed between populations or sexes. All models included interaction terms. All tests were

two-tailed as we had no *a priori* predictions concerning the directionality of possible differences. Means are reported ± standard deviations.

Results

Cortical diaphysis analysis

Figures 1 and 2 illustrate representative long bones of male and female frogs from the core and the edge populations. Differences in the cortical diaphysis are not obvious. The cortical thickness appears to increase with bone length in male and female frogs and differences appear when comparing individuals from the core compared to those from the edge of the range (Figs. 1, 2).

Femur length had a significant impact on the cortical diaphysis (Wilks' lambda = 0.23; $F_{8,24} = 10.29$; $P < 0.001$). The analysis also showed significant population effects (Wilks' lambda = 0.40; $F_{8,24} = 4.45$; $P = 0.002$). The sex effect (Wilks' lambda = 0.59; $F_{8,24} = 2.05$; $P = 0.08$) was marginally non-significant and the interaction between sex and population (Wilks' lambda = 0.78; $F_{8,24} = 0.89$; $P = 0.56$) was not significant. Subsequent ANCOVAs showed differences between males and females (Tables 2, 3) with females typically having larger values than males (e.g. mean total cross-sectional tissue area, mean cross-sectional bone area, mean polar second moment of area). Similarly, differences between populations were significant for all variables except the mean eccentricity (Tables 2, 3) with individuals from the core of the range showing higher values compared to those of the edge of the range.

Bone mineral density

The average BMD for all femora is 1.15 ± 0.08 g/cm3 (Fig 2D, Table 1) with the lowest values being below 1 g/cm3 for two edge samples. There was a significant effect of femur length on bone mineral density ($F_{1,31} = 12.93$; $P = 0.001$; Fig. 2D) with larger bones being more mineralized. The analysis of covariance detected significant sex differences ($F_{1,31} = 5.74$; $P = 0.023$) and differences between populations ($F_{1,31} = 6.12$; $P = 0.019$). The interaction between sex and population was not significant ($F_{1,31} = 0.73$; $P = 0.40$). Inspection of the marginal means showed that

females had a significantly lower bone mineral density than males and that individuals from the edge of the range had lower bone mineral density than those of the core of the range for a given femur length.

Trabecular epiphyses bone analysis

Longitudinal sections of the epiphyses of male and female frogs from the core and edge populations are illustrated in Figure 3. It can be clearly seen that some femora did not show any trabecular bone in neither the proximal nor the distal epiphyses (Supplementary table 1 and supplementary table 4). The trabecular bone parameters analyzed are presented in Figure 4 and supplementary table 4. The BV/TV for the proximal and distal epiphysis ranged from 5% to 25% (Fig. 4; supplementary figure 1). The trabecular thickness in the proximal epiphysis varied between 100 and 150µm, and between 100 µm and 160 µm in the distal epiphysis (Supplementary figure 2). As the trabecular bone observed was mostly present in the distal epiphysis of older individuals (Fig. 3, supplementary table 1), our statistical analysis was restricted to this region.

Femur length significantly impacted the distal trabecular architecture (Wilks' lambda = 0.54; $F_{4,20} = 4.29$; $P = 0.011$). Effects were significant for trabecular volume ($F_{1,23} = 13.31$; $P = 0.001$), bone volume ($F_{1,23} = 16.76$; $P < 0.001$), the ratio of bone volume to trabecular volume ($F_{1,23} = 4.76$; $P = 0.040$), and trabeculae number ($F_{1,23} = 4.47$; $P = 0.046$). However, neither sex (Wilks' lambda = 0.86; $F_{4,20} = 0.82$; $P = 0.53$), population (Wilks' lambda = 0.72; $F_{4,20} = 1.95$; $P = 0.14$), nor their interaction (wilks' lambda = 0.87; $F_{4,20} = 0.76$; $P = 0.56$) impacted the trabecular bone structure. Consequently, neither populations nor sexes differed in the trabecular structure of the distal epiphysis (see also Fig. S1).

Three-point bending analysis

The results from the bending tests are presented in Table 4, Figure 5. The Young's modulus for all samples ranged between 3.27 and 8.5 GPa. On average femoral bone has a high yield strain of 1.6% and failure strain of 7.5% (Fig. 5, Table 4). The MANCOVA showed a significant overall effect of femur length on the biomechanical properties of the femur (Wilks' lambda = 0.19; $F_{7,13} = 7.71$; $P = 0.001$). Whereas population differences were significant (Wilks' lambda = 0.39; $F_{7,13} = 2.91$; $P =$

0.046), differences between sexes were not (Wilks' lambda = 0.53; $F_{7,13} = 1.68$; $P = 0.20$). The interaction between population and sex was also non-significant (Wilks' lambda = 0.85; $F_{7,13} = 0.34$; $P = 0.92$). Subsequent ANCOVAs showed that populations differed significantly in Imin ($F_{1,19} = 17.65$; $P < 0.001$) and diameter ($F_{1,19} = 20.58$; $P < 0.001$). Inspection of the marginal means showed that individuals from the core had a higher minimal principal axis value (i.e. lowest distribution of mass) and diameter compared to those of the edge.

Discussion

The growth of the long bones in frogs differs from that described for mammals and birds in that periosteal ossification dominates with endochondral ossification observed only on the edges of erosion bays at the epiphyses (Fox and Irving, 1950; Dickson, 1982; Felisbino and Carvalho, 2002; Rozenbut and Ogielska 2005; Haines 2008). Cortical thickness changes, on the other hand, are due to the periosteal activity around the diaphysis (Dickson 1982, Dell'Orbo, 1992; Felisbino and Carvalho 1999, 2001; Rozenbut and Ogielska 2005; Erismis and Chinsamy, 2010). Dell'Orbo (1992) stated that bone diameter increased with age without a significant increase in the diameter of the medullary cavity, and concluded that thickening of the diaphyseal cortex was the principal driver of the widening of the diaphysis. We did observe that, independent of variation in size, individuals from the core of the range had a greater cortical thickness compared to edge individuals.

Endochondral ossification has been observed to occur late in the development of aquatic and semi-aquatic frogs and is restricted to the boundary zones of metaphyseal cartilage (Rozenblut and Ogielska 2005; Miura et al. 2008). This late ossification and trabecular bone formation in the epiphyses occur in conjunction with the cessation of bone elongation (Kemp and Hoyt 1969; Felisbino and Carvalho 2001). This is the likely explanation for the absence of trabecular bone in younger individuals in our study. Dell'Orbo et al. (1992) also reported the absence of trabecular bone in *Pelophylax kl. esculentus*. In contrast, some trabecular bone was observed in *Peplophylax caralitanus* from age of six years onwards (Erismis and Chinsamy 2010) with well-developed struts being present in older individuals. Felisbino and Carvalho

(2001) only observed bone trabeculae resulting from endochondral ossification in *Lithobates catesbeianus* that were already almost fully grown, similar to the observations of Rozenblut and Ogielska (2005) in *P. kl. esculentus*. Felisbino and Carvalho (2001) hypothesized that the trabecular formation only occurs with an increased body size and weight in adults, and functions to reinforce the ends of the bones. In accordance, in *X. laevis* we found that the amount of trabecular bone increased with age (i.e., femur length). Moreover, trabecular bone first appeared in the condyle (distal epiphysis) which may reflect the higher mechanical demands on this structure. The earlier onset of the deposition of calcium phosphate in the articular cartilage of the knee joint (distal femur and proximal tibiofibular) observed by Felisbino and Carvallho (2001, 2002) in *Lithobates catesbeianus* also suggests a possible high mechanical stress in this region. Trabecular bone structure was, however, not different between sexes nor between populations suggesting that it is of no advantage to individuals at the edge of range. This may be because trabecular bone develops too late in the ontogeny to be a significant factor in the response of the bone to higher or more frequent loading. Morphologically and functionally the epiphyses of the long bones in frogs are different to those of mammals and birds (e.g., Ruimerman et al. 2005, Pontzer et al. 2006, Barak et al. 2008, 2011; Kivell, 2016) where the formation of trabecular bone enhances the mechanical properties of the bone. Moreover, a consistent relationship between trabecular bone architecture with mechanical properties is not necessarily true and depends on animal location, bone function and mode of loading (e.g. Barak et al. 2010).

Long bone architecture, material, and mechanical properties

The cross-section of the femora of *X. laevis* does not have a visible crest along the length of the diaphysis similar to what has been reported for other aquatic frogs (Vera et al. 2019). However, aquatic and semi-aquatic frogs were predicted by the same authors to have a round diaphysis. The mean eccentricity (0.5) we observed in our CT scans shows that the diaphysis of *X. laevis* is not round but elliptical, with a laterally elongated shape (Fig. 1). It has been hypothesized that a circular geometry is an adaptation to torsion (Broshko, 2014) or multidirectional bending (Demes and Carlson, 2009). A more elliptical cross-section, in contrast, is better suited to resist

bending in one direction. This geometry appears to be conserved as there were no differences between sexes or populations. However, significant differences between core and edge individuals were detected for most other cortical parameters measured. Core and edge individuals differ in muscle mass and muscle cross-sectional area with edge individuals showing more strongly developed muscles (e.g. femur retractor, knee extensor, ankle extensor and flexor, Padilla et al. 2019). Our results show, however, that the cortical bone is thinner, and that edge individuals have lower cortical bone parameters and a lower bone mineral density suggesting that their bones are less resistant to bending. Although this pattern could be indicative of fast locomotion we have no field data on locomotor speed that could test this idea.

In addition to differences between populations we also found significant differences between sexes. Our analysis showed that females have a greater total cross-sectional and cortical bone area as well as greater mean second polar moments of area for a given femur length. In previous studies sex-specific differences in organ size and muscle architecture have been highlighted (Padilla et al. 2019). Interestingly, females had heavier muscles but not a greater physiological muscle cross-sectional area compared to males for a given femur length. Females further invest more energy in reproductive output compared to males (Shine 1979; Courant et al., 2017) and are larger and more corpulent. The greater corpulence of females (i.e., higher weight for a given size) may explain the greater investment in cortical bone, allowing females to resist these greater external forces (body weight) during terrestrial locomotion. This is in accordance with the fact that muscle cross-sectional area does not differ between males and females suggesting that the cortical structure of the femur in *X. laevis* responds mostly to differences in the external (gravitational) forces experienced during terrestrial locomotion.

Bone mineral density has a tight relationship with mechanical properties (e.g. Currey 1990, 1999). Currey (1999), for example has shown a strong relationship of calcium content (proxy for mineral content and comparable in our study with bone density) and Young's modulus (bending strength) in a large sampling of different bone types and species. *Xenopus laevis* females did show a lower bone mineral density (BMD) than males which is reflected in their lower Young's modulus. Edge individuals also had a significantly lower bone mineral density compared to core individuals. BMD

has been shown to improve bone strength (e.g., Turner 2006; Currey, 2002; Ammann and Rizzoli, 2003). In frogs, jumping is mechanically more challenging than swimming (e.g., Lutz and Rome 1994, Calow and Alexander, 1973). Indeed, jumping has been hypothesized to subject frog hind limb bones to high torques requiring a high bone bending strength (e.g., Blob and Biewener, 1999; Blob et al. 2014). Blob and co-authors (2014) showed that *in-vitro* stains measured on the femora of frogs were indeed indicative of bending (e.g., Biewener et al. 1983; Blob and Biewener 1999). Moreover, Wilson et al. (2009) showed that anuran hind limb bones generally show high yield stresses in bending. Our three-point bending experiment shows that the Young's modulus of the femora in *X. laevis* ranges from 3.2 to 8.5 GPa. These values fall within the range observed for fish bone (5-8GPa; Atkins et al. 2014), yet are somewhat lower than values documented for mammalian bone (5-25GPa; Currey 1999, 2002, Shahar et al. 2007). The bending yield stress in *X. laevis* ranged from 55 to 110 MPa and is somewhat lower than values observed and reported for femora of other vertebrates (birds, mammals, reptiles) (96-316 MPa; Currey 1987, Currey 2002, Erickson et al. 2002). The yield strain and stress values recorded here are also somewhat lower than previous data obtained for frogs (Wilson et al., 2019). Differences between the results obtained here and those of previous studies may be due to a variety of factors including differences in the loading rate (lower in our study), the span width used in the three-point bending test, preservation artifacts, the specific set-up used and phylogenetic or ecological differences between species. Future studies would benefit from estimates of in vivo loading rates, adapting the span to the size of the bone, and the use of fresh bone to better understand if the values reported here are good estimates of in vivo whole-bone mechanical properties. Only then will we be able to fully understand their functional and ecological relevance.

Conclusions

Our study showed important differences in the cortical bone geometry between frogs from the core and the edge of the range of an expanding invasive population of *X. laevis*. Moreover, cortical bone structure and bone biomechanics differed significantly between sexes. However, our hypothesis that range edge frogs as well as males would show adaptations to resist higher and more frequent loading was not supported. In

contrast, individuals from the core showed a higher bending resistance compared to individuals from the range edge, possibly due to their relatively higher body mass. As many differences have been observed between core and edge individuals in expanding populations, including for *X laevis*, the fact that edge individuals of this species are able to disperse further and more frequently while they show a lower bending resistance might be explained by a more important behavioral tendency to move in individuals from the range edge.

Acknowledgements

Ron Shahar and Maïtena Dumont would like to thank the Israel Science Foundation (grant # 700/17) for funding this project.

Author contributions

MD and AH conceived the research project. MD led the writing of the manuscript, collecting the data and performing the analyses. MD and JM performed the bending test experiment, analyses were done by MD and RS. AH did the statistical analyses. JC, PP and AH collected the specimens in the field. All authors MD, AH, JC, PP, RS and JM contributed to the interpretation and discussion of the results and editing of the manuscript.

Funding

This work was supported by the Israel Science Foundation (Grant #700/17)

Data availability

all data are presented in the manuscript and its supplementary tables. Ct scans are freely available from the authors upon request.

Conflicts of interest/Competing interests

The authors declare no conflict of interest.

References

Ammann, P. and Rizzoli, R. (2003). Bone strength and its determinants. Osteoporose Int.14(Suppl 3): S13–8.

Atkins, A., Dean, M.N., Habegger, M.L., Motta, P.J., Ofer, L., Repp, F., Shipov, A., Weiner, S., Currey, J.D. and Shahar R. (2014). Anosteocytic bone remodeling challenges paradigms. PNAS 111(45):16047-16052.

Barak, M.M., Weiner, S. and Shahar R. (2008). Importance of the integrity of trabecular bone to the relationship between load and deformation of rat femora: An optical metrology study. Journal of Materials Chemistry 18(32): 3855-3864.

Barak, M.M., Weiner, S. and Shahar, R. (2010). The contribution of trabecular bone to the stiffness and strength of rat lumbar vertebrae. Spine 35(22): E1153-E1159.

Barak, M.M., Lieberman, D.E. and Hublin, J.-J. (2011). A Wolff in sheep's clothing: Trabecular bone adaptation in response to changes in joint loading orientation. Bone 49(6): 1141-1151.

Biewener, A.A., Thomason, J.J., Goodship, A. and Lanyon, L.E. (1983). Bone stress in the horse forelimb during locomotion at different gaits: a comparison of two experimental methods, Journal of Biomechanics 16: 565-76.

Biewener, A.A. and Taylor, R.C. (1986). Bone Strain: A Determinant of Gait and Speed?. J Exp Biol 1 123 (1): 383–400. doi: https://doi.org/10.1242/jeb.123.1.383

Blob, R.W. and Biewener, A.A. (1999). In vivo locomotor strain in the hindlimb bones of *Alligator mississippiensis* and *Iguana iguana*: implications for the evolution of limb bone safety factor and non-sprawling limb posture, J Exp Biol, 1999, vol. 202 (pg. 1023-46)

Blob, R.W., Espinoza, N.R., Butcher, M.T., Lee, A.H., d' Amico, A.R., Baig, F. and Sheffield K.M. (2014). Diversity of Limb-Bone Safety Factors for Locomotion in

Terrestrial Vertebrates: Evolution and Mixed Chains. Integrative and Comparative Biology 54(6): 1058-1071.

Bouxsein, M.L., Boyd, S.K., Christiansen, B.A., Guldberg, R.E., Jepsen, K.J. and Müller, R. (2010). Guidelines for assessment of bone microstructure in rodents using micro–computed tomography. J Bone Miner Res, 25: 1468-1486.

Broshko, Y.O. (2014) Variability of structural and biomechanical parameters of *Pelophylax esculentus* (Amphibia, Anura) limb bones. Vestnik Zoologii, 48, 239–248.

Burton, O.J., Phillips, B.L. and Travis, J.M.J. (2010). Trade-offs and the evolution of life-histories during range expansion. Ecol. Lett.13, 1210–1220.

Calow, L.J. and Alexander, R. McN. (1973). A mechanical analysis of a hind leg of a frog. Journal of the Zoological Society, London 171: 293-321.

Chuang, A. and Peterson, C.R. (2016) Expanding population edges: theories, traits, and trade-offs. Glob Change Biol 22:494–512.

Courant, J., Secondi, J., Bezeiriat, V. and Herrel, A. (2017) Resources allocated to reproduction decrease at the range edge of an expanding population of an invasive amphibian. Biol. J. Linn. Soc. 122: 157-165.

Courant, J., Secondi, J., Guillemet, L., Volette, E. and Herrel, A. (2019a) Rapid changes in dispersal on a small spatial scale at the range edge of an expanding population. Evol. Ecol. 33: 599-612.

Courant, J., Adil, L., de Kegel, B., Adrians, D., Herrel, A. (2019b). Conserved growth rate and age structure of *Xenopus laevis* in the edge and core of an expanding population. *Biological Journal of the Linnean Society*, 128: 122-129.

Currey, J.D. (1987). The evolution of the mechanical properties of amniote bone. J Biomech 20:1035–1044

Currey, J.D. (1990). Physical characteristics affecting the tensile failure properties of compact bone. J. Biomech. 23: 837–844.

Currey, J.D. (1999). What determines the bending strength of compact bone?. J Exp Biol 202 (18): 2495–2503

Currey, J.D. (2002) Bones: Structure and Mechanics (Princeton Univ Press, Princeton, NJ), pp 436.

Dell'Orbo, C., Gioglio, L. and Quacci, D. (1992). Morphology of epiphyseal apparatus of a ranid frog (*Rana esculenta*). Histol Histopathol 7:267-273.

Demes, B. and Carlson, K.J. (2009) Locomotor variation and bending regimes of capuchin limb bones. American Journal of Physical Anthropology, 139, 558–571.

Dickson, R.G. (1982) Ultrastructure of growth cartilage in the proximal femur of the frog, Rana temporaria. J Anat 13

Erickson, G.M., Catanese, J. III. and Keaveny, T,M. (2002). Evolution of the biomechanical material properties of the femur. Anat Rec 268:115–124.

Erismis, U.C. and Chinsamy, A. (2010). Ontogenetic changes in the epiphyseal cartilage of *Rana* (*Pelophylax*) *caralitana* (Anura: Ranidae). The Anatomical Record 293: 1825-1837.

Felisbino, S. L., and Carvalho, H. F. (1999). The epiphyseal cartilage and growth of long bones in Rana catesbeiana. Tissue and Cell, 31(3), 301-307.

Felisbino, S.L. and Carvalho, H.F. (2001). Growth cartilage calcification and formation of bone trabeculae are late and dissociated events in the endochondral ossification of *Rana catesbeiana*. Cell Tissue Research 306: 919-923.

Felisbino, SL. and Carvalho, H.F. (2002). Ectopic mineralization of articular cartilage in the bullfrog *Rana catesbeaina* and its possible involvement in bone closure. Cell Tissue Research 307: 357-365.

Fox, E. and Irving J. The ossification process in the long bones of *Xenopus laevis*. S Afr J Med Sci 1950;15:5–10.

Fouquet, A. (2001) Des clandestins aquatiques. Zamenis 6: 10-11.

Haines, R.W. (2008) The evolution of epiphyses and of endochondral bone. Biol Rev Cambridge Phil Soc 1942;17:25.

Kemp, N.E. and Hoyt, J.A. (1969): Sequence of ossification in the skeleton of growing and metamorphosing tadpoles of *Rana pipiens*. Journal of Morphology 129: 415-444.

Kivell, T.L. (2016). A Review of Trabecular Bone Functional Adaptation: What Have We Learned From Trabecular Analyses in Extant Hominoids and What Can We Apply to Fossils? Journal of Anatomy 228(4):569-594.

Kular, J., Tickner, J., Chim, S. and Xu, J. (2012) An overview of the regulation of bone remodelling at the cellular level. Clin. Biochem. 45, 863–873.

Linde, F. and Sorensen, H.C.F. (1993). The effect of different storage methods on the mechanical properties of trabecular bone. Journal of Biomechanics 26(10): 1249-1252.

Louppe, V., Courant, J., and Herrel, A. (2017). Differences in mobility at the range edge of an expanding invasive population of *Xenopus laevis* in the West of France? The Journal of Experimental Biology 220: 278–283.

Louppe, V., Courant J, Videlier, M., and Herrel, A. (2018). Differences in standard metabolic rate at the range edge versus the center of an expanding invasive population of *Xenopus laevis* in the West of France. Journal of Zoology 305: 163–172.

Lutz, G.J. and Rome, L.C. (1994) Built for jumping: the design of the frog muscular system. Science, 263, 370–372.

Measey, G.J., Rödder, D., Green, S.L., Kobayashi, R., Lillo, F., Lobos, G., Rebelo, R. and Thirion, J.-M. (2012) Ongoing invasions of the African clawed frog, *Xenopus laevis*: a global review. Biol. Invasions 14: 2255-2270.

Miura S., Hanaoka K. and Togashi S. (2008). Skeletogenesis in *Xenopus tropicalis*: Characteristic bone development in an anuran amphibian. Bone 43: 901-909.

Mollot, G., Pantel, J.H. and Romanuk, T.N. (2017) The effects of invasive species on the decline in species richness: a global meta-analysis. In: Networks of invasion: a synthesis of concepts (D.A. Bohan, A.J. Dumbrell and F. Massol Eds.). Advances in Ecological Research 56: 61-83.

Padilla, P., Courant, J., and Herrel, A. (2019). Allocation trade-offs impact organ size and muscle architecture in an invasive population of *Xenopus laevis* in Western France. J Anat. 235(6):1057-1064.

Philips, B.L., Brown, G.P., Webb, J.K. and Shine, R. (2006). Invasion and the evolution of speed in toads. Nature 439: 803.

Pontzer, H., Lieberman, D.E., Momin, E., Devlin, M.J., Polk J.D., Hallgrimsson B. and Cooper, D.M.L. (2006). Trabecular bone in the bird knee responds with high sensitivity to changes in load orientation. Journal of experimental biology 209: 57-65.

Prikryl, T., Aerts, P., Havelková, P., Herrel, A. and Rocek, Z. (2009) Pelvic and thigh musculature in frogs (Anura) and origin of anuran jumping locomotion. J. Anat. 214: 100-139.

Rozenblut, B. and Ogielska, M. (2005). Development and Growth of Long Bones in European Water Frogs (Amphibia: Anura: Ranidae), With Remarks on Age Determination. Journal of morphology 265: 304-317.

Ruimerman, R., van Rietbergen, B., Hilbers, P. and Huiskes, R. (2005). The effects of trabecular bone loading variables on the surface signaling potential for bone remodeling and adaptation. Annals of biomedical engineering 33: 71-78.

Shahar, R., Zaslansky, P., Barak. M., Friesem, A. A., Currey, J. D. and Weiner, S. (2007). Anisotropic Poisson's ratio and compression modulus of cortical bone determined by speckle interferometry. J. Biomech. 40, 252-264.

Sharir, A., Barak, M. M. and Shahar, R. (2008). Whole bone mechanics and mechanical testing. The Veterinary Journal 177: 8-17.

Shine, R. (1979) Sexual selection and sexual dimorphism in the Amphibia. Copeia 2: 297-306

Shine, R., Brown, G.P. and Phillips, BL. (2011) An evolutionary process that assembles phenotypes through space rather than through time. Proc. Natl. Acad. Sci. USA 108:5708–5711.

Simberloff, D., Martin, J-L., Genovesi, P., Maris,V., Wardle, D.A., Aronson, J., Courchamp, F., Galil, B., Garcia-Berthou, E., Pascal, M., Pysek, P., Sousa, R., Tabacchi, E. and Vila M. (2013) Impacts of biological invasions: what's what and the way forward. Trends Ecol. Evol. 28: 58-66.

Stoltz, J-F., Magdalou, J., George, D., Chen, Y., Li, Y., De Isla, N., He, X. and Remond, Y. (2018) Influence of mechanical forces on bone: Introduction to mechanobiology and mechanical adaptation concept. J. Cell Immunother. 4: 10-12.

Tingley, R., Vallinoto, M., Sequeira, F. and Kearney, MR. (2014). Realized niche shift during a global biological invasion. Proc. Natl. Acad. Sci. U.S.A. 111:10233–10238.

Tinsley, R., Minter, L., Measey J, et al. (2009) Xenopus laevis. The IUCN Red List of Threatened Species 2009: e.T58174A11730010. https://doi.org/10.2305/iucn.uk.2009.rlts. t58174a11730010.en.

Turner, C.H. and Burr, D.B. (1993). Basic biomechanical measurements of bone: a Tutorial. Bone 14(4): 595-608.

Turner, C. H. (2006). Bone strength: current concepts Skeletal Development and Remodeling in Health, Disease, and Aging (Annals of the New York Academy of Sciences) vol 1068 (New York: New York Academy of Sciences) pp 429-46

Vera, M.C., Ferretti J.-L. and Abdala, V. (2020). Biomechanical properties of anuran long bones correlations with locomotor modes and habitat use. Journal of anatomy 236: 1112-1125.

Vesper, E.O., Hammond, A., Allen, M.R. and Wallace, J.M. (2017). Even with rehydration, preservation in ethanol influences the mechanical properties of bone and how bone responds to experimental manipulation. Bone 97: 49-53.

Vimercati, G., Labadesse, M., Dejean, T. and Secondi, J. (2020) Assessing the effect of landscape features on pond colonisation by an elusive amphibian invader using environmental DNA. Freshwater Biol. 65: 502-513.

Wilson, M.P., Espinoza, N.R., Shah, S.R. and Blob, R.W. (2009), Mechanical Properties of the Hindlimb Bones of Bullfrogs and Cane Toads in Bending and Torsion. Anat Rec, 292: 935-944.

Figures and Tables

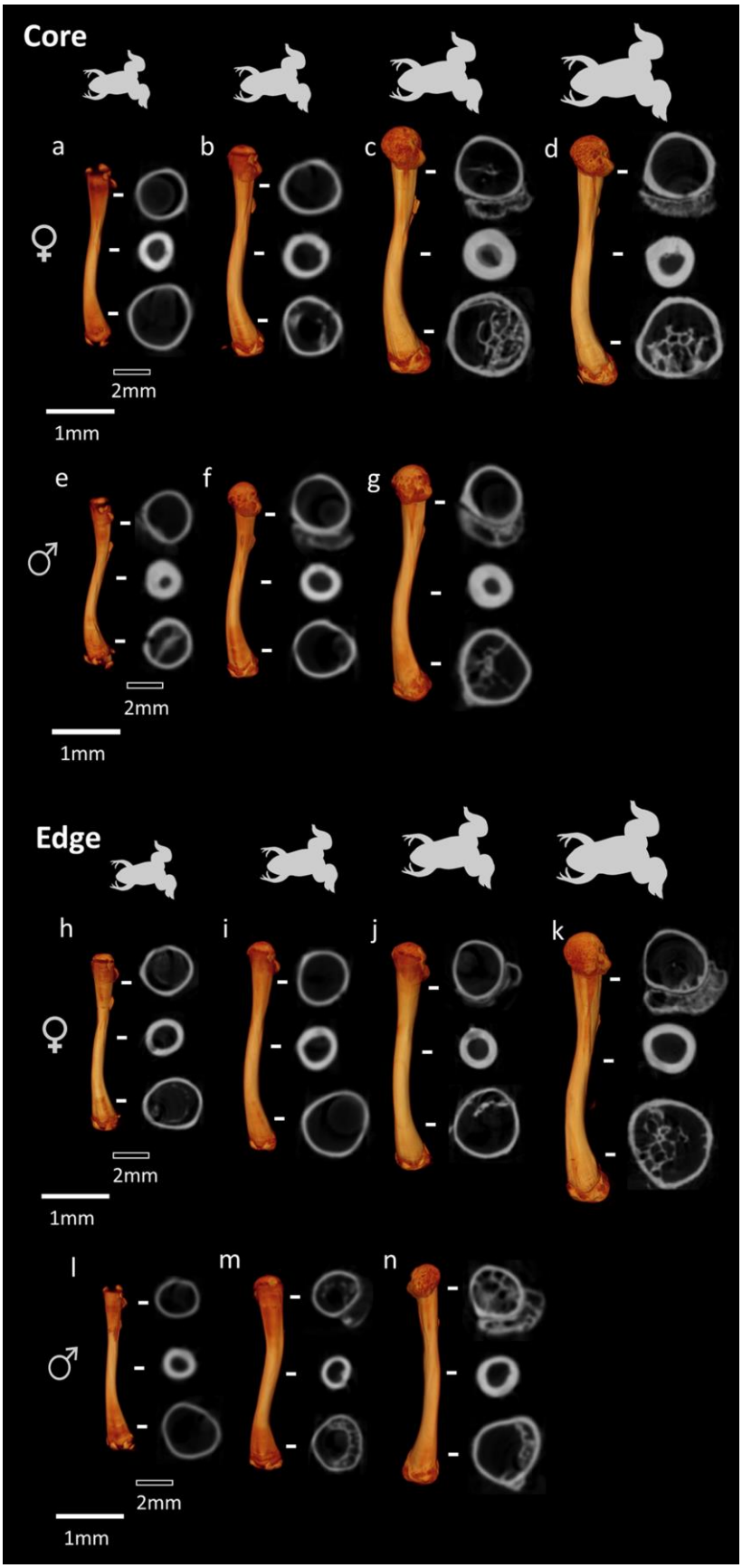

Fig. 1. Reconstructions of selected representative femurs from individuals of increasing size for each of the groups (a-d: female core; e-g: male core; h-k: female edge; l-n: male edge). Corresponding cross sections have been added to show details of cortical bone at three locations in each bone indicated by the white horizontal stripes. The specimens used for this image (Specimen number (femora length in mm) were: a: C15 (25mm), b: C24 (32.42mm), c: C26 (36.34mm), d: C8 (42.22mm); male core e: C44 (25.58mm), f: C29 (26.24mm), g: C38(33.3mm); female edge: h: E6 (28.55mm), i: E7 (31.7mm), j: E15 (33.47mm), k: E16 (43.27mm); male edge: l: E25 (24.69mm), m: E28 (28.8mm), n: E14 (33.33mm). Scale bars: White = 1.0 mm corresponding to the images of the bones; black = 2.0 mm corresponding to the bone cross-sections.

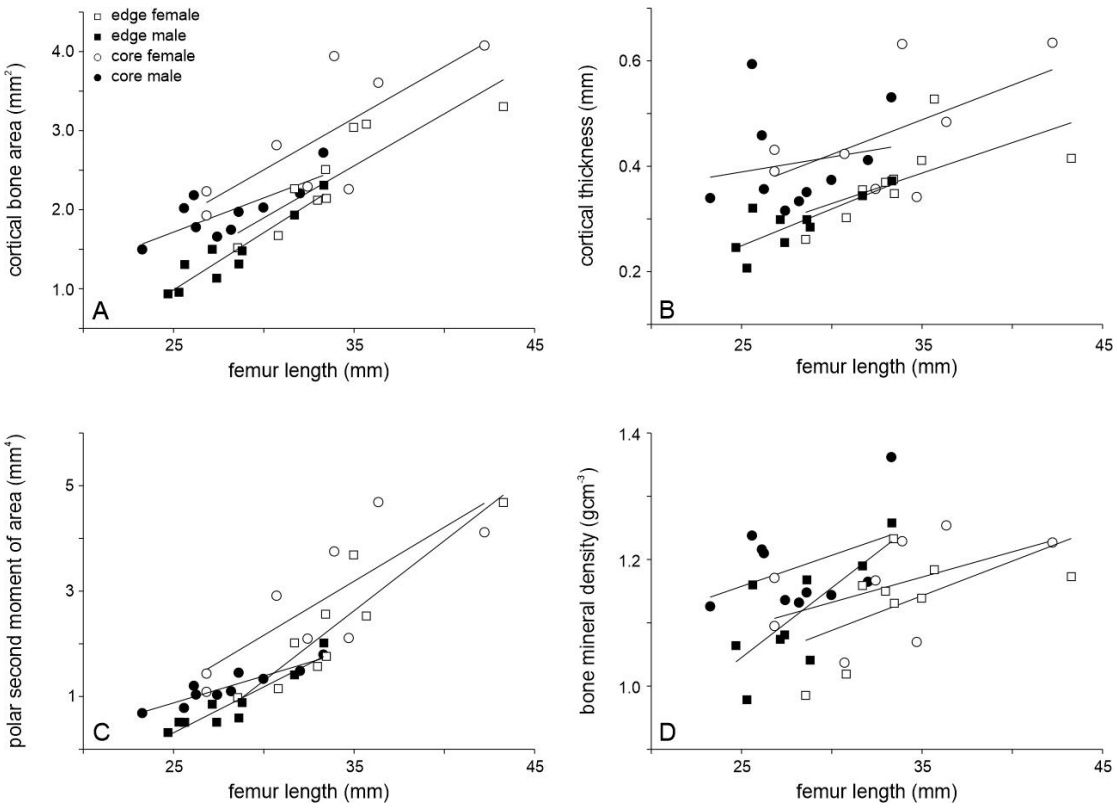

Fig. 2. Comparison of selected cortical bone parameters as a function of femoral length between the edge (E/square) and core (C/circle) populations for males (black) and females (white). A. Cross-sectional bone area (mm^2), B. Cortical thickness (mm), C. Mean polar second moment of area (mm^4), D. BMD, bone mineral density (g/cm^3). Trend lines have been added to the graph. See supplementary table 1 for the raw data.

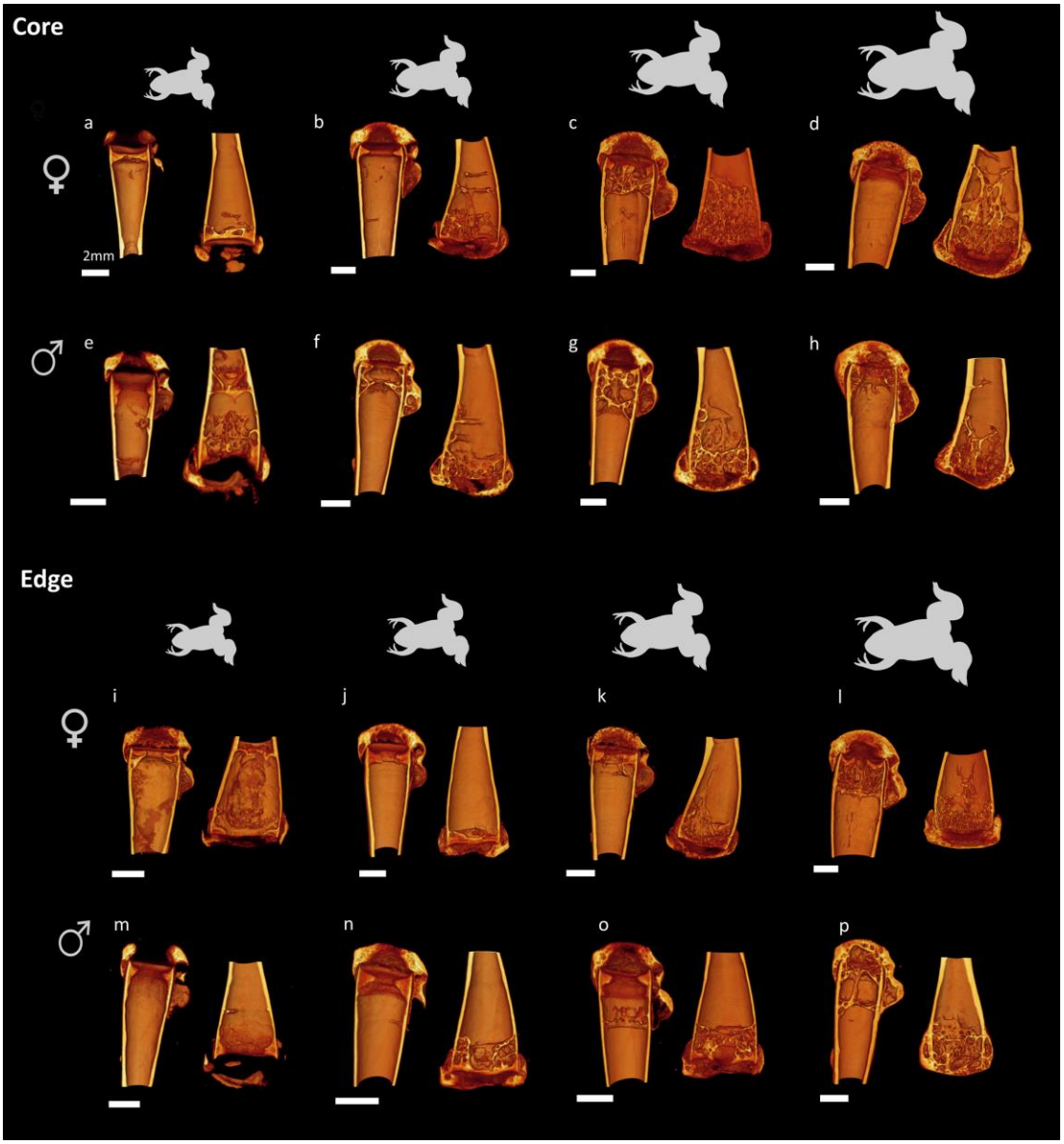

Fig. 3. Illustration of the trabecular bone present in a longitudinal cut of the proximal (left) and distal (right) epiphyses of selected *Xenopus laevis* femora for the core population (top) and edge (down) for each sex, ranked by increasing femur length (from left to right). Female core (in brackets femur length in mm): a: C15 (26.82mm), b: C24 (32.42mm), c: C23 (33.9mm), d: C8 (42.22mm); Male core: e: C44 (25.58mm), f: C29 (26.24mm), g: C11 (32mm), h: C38 (33.3mm). Female edge: i: E6 (28.55mm), j: E7 (31.7mm), k: E15 (33.47mm), l: E16 (43.27mm); Male edge: m: E25 (24.69mm), n: E17 (27.39mm), o: E28 (28.8mm), p: E14 (33.33m).

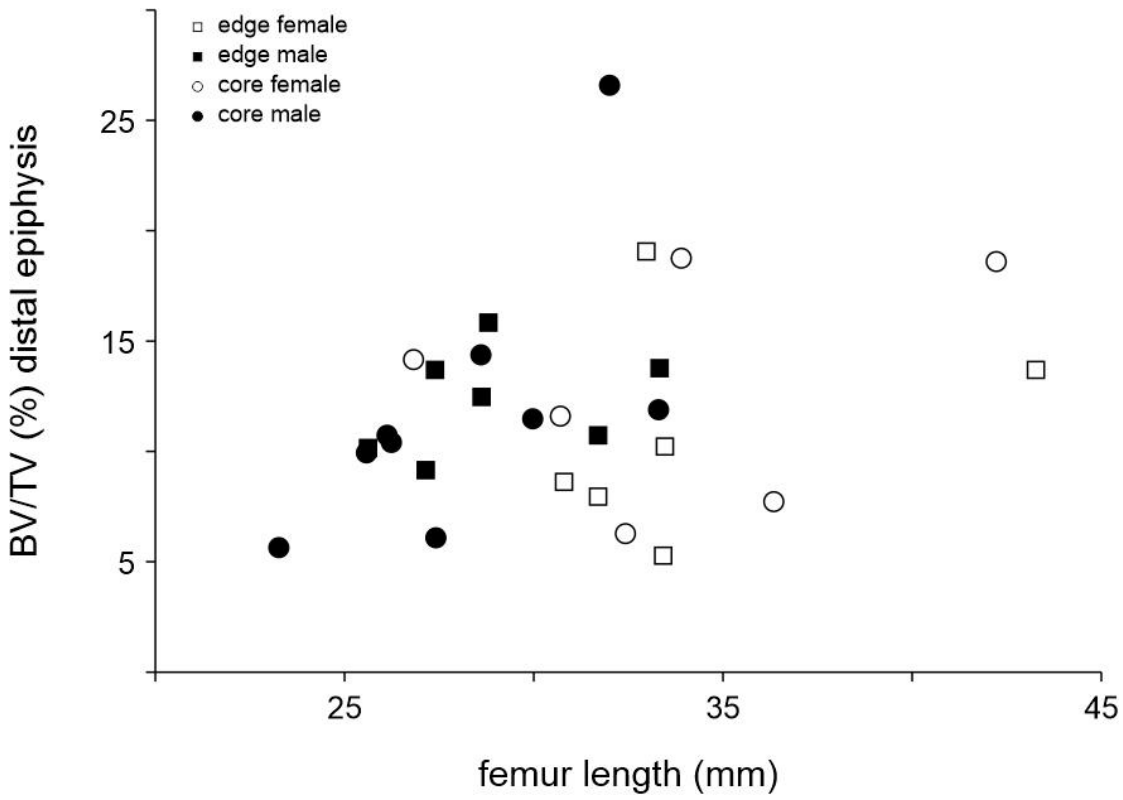

Fig. 4. Scatterplot of bone volume relative to total tissue volume (BV/TV, in %) against femur length (mm) for the distal epiphyses of *Xenopus laevis* femora. Edge individuals are represented by squares and core individuals by circles. Males are indicated in black and females in white. Raw data can be found in supplementary table 6.

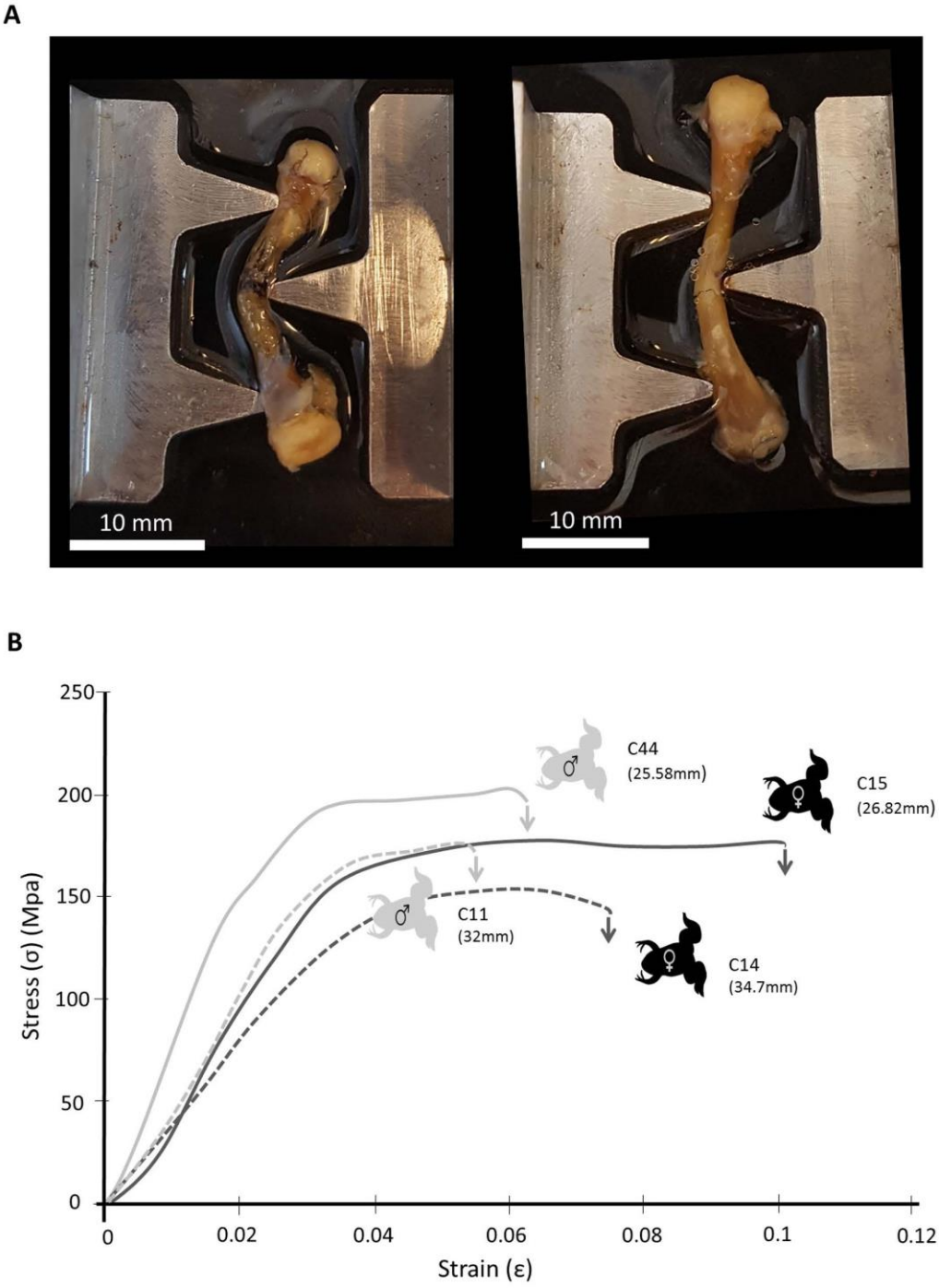

Fig. 5. A. Picture of three-point bending test of a femur harvested from a male (left: individual C44; femur length of 25.6mm) and female (right: individual C26; femur length of 36.34mm). **B.** Graph of the strain/stress curves for four representative femora: males are indicated in grey, females in black. The dashed lines represent larger individuals and the full lines smaller ones. Femur lengths are indicated below the individual number. C = core; E = edge. Raw data can be found in table 3.

Table 1. Different cortical parameters obtained for the cortical bone of femoral diaphysis in *Xenopus laevis*.

Individual	sex	Femur length (mm)	T.Ar (mm^2)	B.Ar (mm2)	MMI(polar) (mm^4)	Av.MMI(max) (mm^4)	Av.MMI(min) (mm^4)	Ecc	Cs.Th (mm)	BMD (g/cm^3)	
										mean	stdev
C20	M	23.2	2.23	1.50	0.69	0.39	0.29	0.51	0.34	1.12	0.12
C8	F	42.2	5.24	4.08	4.12	2.21	1.91	0.36	0.63	1.23	0.11
C14	F	34.7	4.11	2.26	2.11	1.13	0.98	0.36	0.34	1.07	0.1
C23	F	33.9	5.01	3.94	3.75	2.01	1.74	0.37	0.63	1.23	0.1
C6	M	28.6	3.33	1.97	1.45	0.82	0.63	0.49	0.35	1.15	0.17
C9	F	26.8	2.80	1.93	1.09	0.60	0.49	0.43	0.39	1.17	0.13
C11	M	32.0	3.25	2.21	1.49	0.80	0.69	0.37	0.41	1.16	0.16
C12	F	30.7	4.69	2.82	2.91	1.54	1.37	0.33	0.42	1.04	0.13
C13	M	30.0	3.13	2.03	1.34	0.80	0.54	0.57	0.37	1.14	0.16
C15	F	26.8	3.14	2.23	1.43	0.80	0.64	0.44	0.43	1.09	0.17
C24	F	32.4	4.12	2.29	2.10	1.11	0.99	0.31	0.36	1.16	0.13
C26	F	36.3	5.93	3.61	4.69	2.48	2.20	0.34	0.48	1.22	0.14
C27	M	26.1	2.85	2.18	1.20	0.66	0.54	0.43	0.46	1.22	0.14
C29	M	26.2	2.74	1.78	1.04	0.56	0.48	0.37	0.36	1.21	0.16
C38	M	33.3	3.47	2.72	1.80	0.95	0.84	0.34	0.53	1.36	0.13
C41	M	27.4	2.82	1.66	1.03	0.55	0.48	0.35	0.32	1.13	0.12
C44	M	25.6	2.24	2.02	0.78	0.45	0.33	0.52	0.59	1.24	0.11
C46	M	28.2	2.89	1.75	1.10	0.52	0.51	0.37	0.33	1.13	0.11
E13	F	35.7	4.13	3.08	2.53	1.43	1.10	0.48	0.53	1.18	0.11

E15	F	33.5	3.74	2.14	1.76	0.92	0.84	0.29	0.35	1.13	0.11
E16	F	43.3	6.12	3.30	4.68	2.68	2.00	0.50	0.46	1.17	0.11
E2	F	33.0	3.43	2.12	1.57	0.87	0.70	0.44	0.37	1.15	0.11
E6	F	28.6	2.86	1.52	0.98	0.55	0.43	0.45	0.26	0.99	0.12
E10	M	25.3	2.20	0.96	0.51	0.31	0.20	0.59	0.21	0.98	0.1
E1	F	35.0	5.46	3.04	3.69	2.17	1.52	0.55	0.41	1.14	0.12
E7	F	31.7	4.02	2.27	2.02	1.08	0.94	0.34	0.36	1.16	0.14
E8	M	25.6	1.91	1.31	0.51	0.28	0.23	0.43	0.32	1.16	0.1
E11	F	33.4	4.50	2.51	2.56	1.47	1.09	0.51	0.38	1.23	0.13
E12	M	31.7	3.29	1.93	1.41	0.75	0.66	0.35	0.34	1.19	0.15
E14	M	33.3	3.96	2.31	2.02	1.11	0.91	0.42	0.37	1.26	0.14
E17	M	27.4	2.01	1.13	0.51	0.29	0.23	0.46	0.26	1.08	0.11
E22	M	28.6	2.09	1.31	0.59	0.32	0.27	0.41	0.30	1.17	0.14
E25	M	24.7	1.54	0.94	0.32	0.17	0.14	0.42	0.25	1.06	0.09
E27	F	30.8	3.03	1.67	1.15	0.63	0.52	0.43	0.30	1.02	0.12
E28	M	28.8	2.66	1.48	0.88	0.51	0.38	0.51	0.28	1.04	0.12
E29	M	27.2	2.54	1.50	0.85	0.46	0.39	0.40	0.30	1.07	0.13

T.Ar = Tissue area; B.Ar = Bone area; MMI = Mean polar moment of inertia; Av.MMI(max) = average principal moment of inertia (max); Av.MMI(min) = average principal moment of inertia (min); Ecc = mean eccentricity; Cs.Th = cross-sectional thickness, BMD= bone mineral density (mean and stdev=standard deviation).

Table 2. results of the univariate analyses of covariance.

Effect tested	variable	$F_{1,31}$	P
femur length	Mean total cross-sectional tissue area (mm^2)	76.98	< **0.001***
	Bone mineral density (g/cm^3)	12.93	**0.001***
	Mean cross-sectional bone area (mm^2)	60.30	< **0.001***
	Mean polar second moment of area (mm^4)	87.43	< **0.001***
	Average principal second moment of area (max.) (mm^4)	80.40	< **0.001***
	Average principal second moment of area (min.) (mm^4)	91.72	< **0.001***
	Eccentricity	1.55	0.222
	Cross-sectional thickness (mm)	12.00	**0.002***
sex	Mean total cross-sectional tissue area (mm^2)	9.86	**0.004***
	Bone mineral density	5.74	**0.023**
	Mean cross-sectional bone area	4.65	**0.039**
	Mean polar second moment of area	9.33	**0.005***
	Average principal second moment of area (max.)	8.61	**0.006***
	Average principal second moment of area (min.)	9.81	**0.004***
	Eccentricity	0.11	0.740
	Cross-sectional thickness	0.13	0.724
population	Mean total cross-sectional tissue area	11.56	**0.002***
	Bone mineral density	6.11	**0.019**
	Mean cross-sectional bone area	32.49	< **0.001***
	Mean polar second moment of area	20.08	< **0.001***
	Average principal second moment of area (max.)	17.01	< **0.001***
	Average principal second moment of area (min.)	23.16	< **0.001***
	Eccentricity	3.77	0.061
	Cross-sectional thickness	21.46	< **0.001***
sex * pop	Mean total cross-sectional tissue area	0.85	0.364
	Bone mineral density	0.73	0.400

Mean cross-sectional bone area	1.42	0.242
Mean polar second moment of area	1.11	0.301
Average principal second moment of area (max.)	1.50	0.231
Average principal second moment of area (min.)	0.64	0.430
Eccentricity	1.99	0.169
Cross-sectional thickness	0.61	0.441

Bolded P-values highlight significant differences; asterisks highlight significant differences after sequential Bonferroni correction for multiple testing.

Table 3. marginal means for the cortical parameters derived from the ANCOVAs.

Variable	sex	pop.	Mean	Std. Error	95% Confidence Interval	
Mean total cross-sectional tissue area (mm^2)	F	C	0.574	0.021	0.532	0.617
		E	0.527	0.021	0.485	0.57
	M	C	0.517	0.019	0.478	0.556
		E	0.435	0.02	0.394	0.476
Bone mineral density (g/cm^3)						
	F	C	0.052	0.01	0.032	0.071
		E	0.038	0.01	0.018	0.057
	M	C	0.085	0.009	0.067	0.103
		E	0.056	0.009	0.038	0.075
Mean total cross-sectional tissue perimeter (mm)	F	C	0.863	0.011	0.841	0.884
		E	0.840	0.01	0.818	0.861
	M	C	0.834	0.01	0.814	0.854
		E	0.794	0.01	0.774	0.815
Mean cross-sectional bone area (mm^2)	F	C	0.388	0.025	0.337	0.438
		E	0.287	0.025	0.237	0.337
	M	C	0.354	0.023	0.308	0.4
		E	0.199	0.024	0.151	0.248
Mean total cross-sectional bone perimeter (mm)	F	C	1.065	0.016	1.032	1.098
		E	1.064	0.016	1.032	1.097
	M	C	1.023	0.015	0.993	1.053
		E	1.009	0.015	0.978	1.041
Mean polar second moment of area (mm^4)	F	C	0.283	0.04	0.201	0.365
		E	0.158	0.04	0.077	0.24
	M	C	0.182	0.037	0.107	0.257
		E	-0.019	0.038	-0.098	0.059
Average principal second moment of area (max.) (mm^4)	F	C	0.015	0.041	-0.069	0.1
		E	-0.093	0.041	-0.177	-0.009
	M	C	-0.076	0.038	-0.153	0.001
		E	-0.276	0.039	-0.356	-0.195
Average principal second moment of area (min.) (mm^4)	F	C	-0.054	0.04	-0.136	0.027
		E	-0.200	0.04	-0.281	-0.119
	M	C	-0.167	0.037	-0.242	-0.093
		E	-0.371	0.038	-0.449	-0.293

Eccentricity						
	F	C	-0.428	0.027	-0.483	-0.373
		E	-0.346	0.027	-0.401	-0.291
	M	C	-0.383	0.025	-0.434	-0.333
		E	-0.370	0.026	-0.423	-0.317
Cross-sectional thickness (mm)						
	F	C	-0.376	0.029	-0.435	-0.318
		E	-0.477	0.029	-0.535	-0.418
	M	C	-0.368	0.026	-0.421	-0.314
		E	-0.509	0.028	-0.565	-0.453

Covariates appearing in the model are evaluated at a femur length = 1.48. C = core; E = Edge; F = female; M = male; Pop = population.

Table 4. Results of the bending analysis showing the raw data for each individual.

Individual	**Femur length** (mm)	**Average moment of inertia** (mm^4)	**Cross sectional mid-diaphysis diameter** (mm)	**Young's modulus** (Gpa)	**yield stress σ** (N/mm^2)	**yield strain ε**	**Ultimate stress** (N/mm^2)	**Ultimate strain**
Core males								
C6	28.6	0.68	2.11	5.70	73.03	0.013	137.04	0.064
C11	32.0	0.71	1.98	6.31	83.41	0.017	168.42	0.055
C44	25.6	0.33	1.65	8.49	110.14	0.014	188.03	0.063
C46	28.2	0.54	1.96	6.92	98.18	0.018	168.05	0.109
C13	30.0	0.54	2.00	6.82	92.37	0.011	158.63	0.046
C29	26.2	0.48	1.80	7.81	90.50	0.012	84.67	0.109
Core females								
C23	33.9	1.87	2.41	5.35	88.24	0.028	171.93	0.075
C26	36.3	2.28	2.86	4.11	76.44	0.020	151.62	0.046
C14	34.7	0.98	2.42	5.20	54.57	0.013	142.96	0.075
C15	26.8	0.65	1.95	6.01	80.02	0.017	172.04	0.101
C9	26.8	0.49	1.83	4.55	72.19	0.019	126.19	0.048
C12	30.7	1.39	2.5	3.27	53.57	0.018	92.00	0.115
Edge males								
E28	28.8	0.40	1.74	4.77	61.53	0.025	131.87	0.071
E8	25.6	0.24	1.66	8.52	110.91	0.014	229.29	0.073
E14	33.3	0.97	2.21	7.04	91.51	0.018	171.73	0.050
E12	31.7	0.67	1.91	6.64	73.24	0.013	100.73	0.093

E22	28.6	0.29	1.59	8.34	85.56	0.011	80.61	0.120
E29	27.2	0.39	1.65	6.67	83.39	0.011	127.13	0.071
Edge females								
E7	31.7	0.95	2.22	5.32	77.122	0.015	140.69	0.080
E27	30.8	0.57	1.83	4.96	65.244	0.013	126.74	0.059
E15	33.5	0.88	2.14	5.35	81.167	0.015	148.30	0.096
E13	35.7	1.12	2.26	5.26	59.81	0.013	180.19	0.083
E2	33.0	0.76	2.00	5.29	58.05	0.013	124.20	0.060
E6	29.0	0.43	1.87	7.25	81.54	0.014	171.22	0.041

C = Core; E = Edge

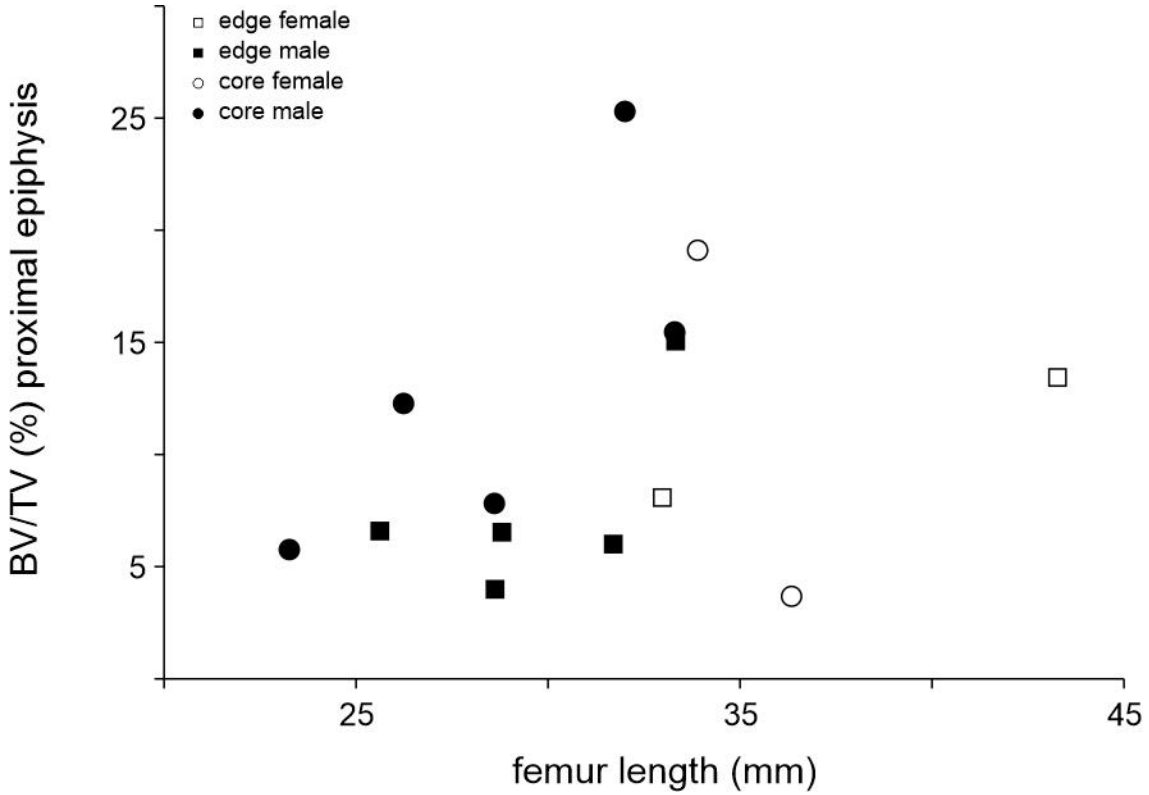

Fig. S1. Bone volume relative to total tissue volume in the proximal epiphysis of *Xenopus laevis* in function of femur length. Black symbols represent males, white symbols represent females. Squares represent edge individuals, circles represent core individuals.

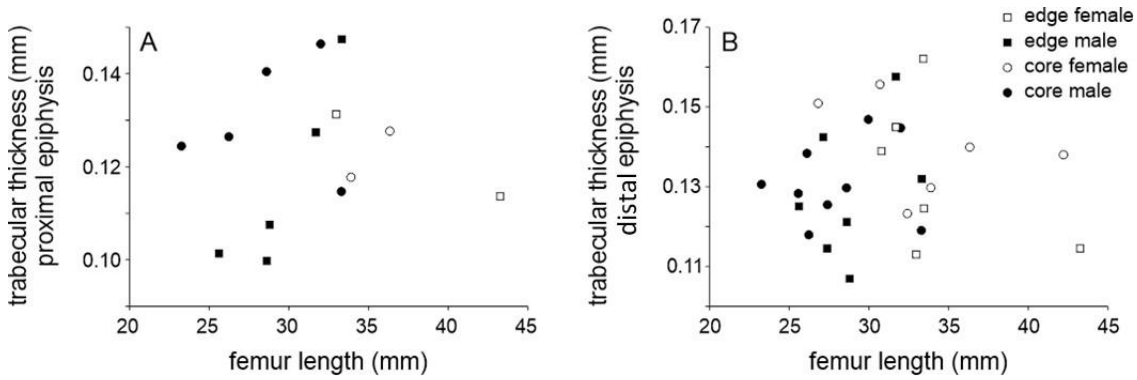

Fig. S2. Trabecular thickness in the proximal (A) and distal (B) epiphyses of *Xenopus laevis* in function of femur length. Black symbols represent males, white symbols represent females. Squares represent edge individuals, circles represent core individuals.

Table S1. Table summarizing the presence/absence of trabecular bone in the epiphyses in *Xenopus laevis* femora. Individuals are ranked according to their length. Grey colored cells highlight individuals with no or few trabeculae; black colored cells highlight individuals with many trabeculae. Only individuals indicated in black were used in the quantitative analysis.

Core males																		
Individual	C20	C41	C44	C27	C29			C46	C6		C13	C11		C38				
Femur length (mm)	23.2	25.2	25.5	26.1	26.2			28.1	28.6		29.9	32.0		33.3				
Anterior epiphysis																		
Posterior epiphysis																		
Core females																		
Individual					C15	C9					C12	C24			C23	C14	C26	C8
Femur length (mm)					26.8	26.8					30.7	32.4			33.9	34.7	36.3	42.2
Anterior epiphysis																		
Posterior epiphysis																		
Edge males																		
Individual	E25	E10	E8				E17	E29	E22	E28		E12		E14				
Femur length (mm)	24.6	25.3	25.6				27.3	27.6	28.6	28.8		31.7		33.3				
Anterior epiphysis																		
Posterior epiphysis																		
Edge females																		
Individual									E6		E27	E7	E2	E11	E15	E1	E13	E16
Femur length (mm)									28.5		30.8	31.7	32.9	33.4	33.4	34.9	35.6	43.2
Anterior epiphysis																		
Posterior epiphysis																		

C = Core; E = Edge

Table S2. Tests of normality for the Log_{10}-transformed variables.

	Shapiro Wilk	d.f.	*P*
Femur length (mm)	0.948	11	0.61
Mean total cross-sectional tissue area (mm^2)	0.964	11	0.82
Mean total cross-sectional bone area (mm^2)	0.916	11	0.29
Cross-sectional thickness (mm)	0.896	11	0.17
Mean polar moment of inertia (mm^4)	0.953	11	0.69
Average maximal principal moment of inertia (mm^4)	0.956	11	0.72
Average minimal principal moment of inertia (mm^4)	0.952	11	0.67
Eccentricity	0.953	11	0.68
Tissue volume - distal (mm^3)	0.938	11	0.49
Bone volume - distal (mm^3)	0.991	11	1.00
Bone volume/tissue volume - distal (%)	0.981	11	0.97
Trabecular thickness - distal (mm)	0.990	11	1.00
Trabeculae number - distal (mm^{-1})	0.967	11	0.85
Trabecular separation - distal (mm)	0.986	11	1.00
Bone mineral density (g/cm^3)	0.896	11	0.17
Average moment of inertia (mm^4)	0.954	11	0.70
Cross sectional mid-diaphysis diameter (mm)	0.958	11	0.74
Young's modulus (GPa)	0.934	11	0.45
Yield stress σ (N/mm^2)	0.907	11	0.23
Yield strain $\boldsymbol{\varepsilon}$	0.861	11	0.06
Ultimate stress (N/mm2)	0.954	11	0.69
Ultimate strain	0.958	11	0.74

Table S3. Results of the Levene's tests for homogeneity of variance

	F	d.f.	*P*
Mean total cross-sectional tissue area (mm^2)	1.918	3,32	0.147
Mean total cross-sectional bone area (mm^2)	0.682	3,32	0.570
Cross-sectional thickness (mm)	0.890	3,32	0.457
Mean polar moment of inertia (mm^4)	2.038	3,32	0.128
Average maximal principal moment of inertia (mm^4)	1.999	3,32	0.134
Average minimal principal moment of inertia (mm^4)	2.375	3,32	0.088
Eccentricity	1.286	3,32	0.296
Bone mineral density (g/cm^3)	0.074	3,32	0.973
Tissue volume - distal (mm^3)	3.200	3,7	0.093
Bone volume - distal (mm^3)	1.381	3,7	0.325
Bone volume/tissue volume - distal (%)	5.344	3,7	0.031
Trabecular thickness - distal (mm)	3.751	3,7	0.068
Trabeculae number - distal (mm^{-1})	2.400	3,7	0.153
Trabecular separation - distal (mm)	2.006	3,7	0.202
Average moment of inertia (mm^4)	1.228	3,7	0.369
Cross sectional mid-diaphysis diameter (mm)	0.598	3,7	0.636
Young's modulus (GPa)	0.852	3,20	0.482
Yield stress σ (N/mm^2)	3.242	3,20	0.044
Yield strain **ε**	1.319	3,20	0.296
Ultimate stress (N/mm2)	0.852	3,20	0.482
Ultimate strain	0.196	3,20	0.898

Note that yield stress does not show homogeneity of variance.

Table S4. Trabecular variables for the anterior and posterior epiphyses of *Xenopus laevis* femora.

Ind	Tissue volume (mm^3)	Bone volume (mm^3)	BV/TV (%)	Trabecular thickness (mm)	Trabeculae number (mm^{-1})	Trabecular separation (mm)
Proximal epiphysis						
C20	4.91	0.28	5.76	0.12	0.46	0.86
C6	3.48	0.27	7.82	0.14	0.56	0.64
C11	10.11	2.56	25.29	0.15	1.73	0.56
C29	5.21	0.64	12.27	0.13	0.97	0.58
C38	6.84	1.06	15.46	0.12	1.35	0.71
C23	11.19	2.14	19.10	0.12	1.62	0.38
C26	19.2	0.72	3.67	0.13	0.29	2.16
E16	15.82	2.13	13.44	0.11	1.18	0.47
E2	6.61	0.53	8.08	0.13	0.62	1.10
E8	2.35	0.16	6.58	0.10	0.65	0.71
E12	2.68	0.16	6.01	0.13	0.47	0.51
E14	10.49	1.58	15.06	0.15	1.02	0.82
E22	1.70	0.07	3.99	0.10	0.40	0.46
E28	3.31	0.22	6.53	0.11	0.61	0.60
Distal epiphysis						
C20	6.41	0.36	5.64	0.13	0.43	1.10
C6	14.44	2.08	14.37	0.13	1.11	0.67
C11	21.19	5.63	26.58	0.15	1.84	0.65
C13	10.59	1.22	11.47	0.15	0.78	0.99
C27	17.78	1.91	10.73	0.14	0.78	1.27
C29	15.52	1.62	10.41	0.12	0.88	0.82
C38	23.29	2.77	11.89	0.12	1.00	0.79
C41	7.61	0.46	6.09	0.13	0.49	0.90
C44	8.49	0.84	9.93	0.13	0.77	0.86
C8	41.26	7.67	18.60	0.14	1.35	0.68
C23	49.78	9.34	18.75	0.13	1.45	0.67
C9	4.90	0.69	14.16	0.15	0.94	0.58
C12	14.43	1.67	11.59	0.16	0.75	0.86
C24	29.54	1.85	6.27	0.12	0.51	1.34
C26	54.63	4.22	7.72	0.14	0.55	1.26
P15	14.03	1.43	10.22	0.13	0.82	1.09
E16	43.34	5.93	13.69	0.12	1.20	0.57
E2	16.91	3.22	19.06	0.11	1.69	0.51
E7	5.30	0.42	7.95	0.15	0.55	0.55
E11	13.64	0.72	5.28	0.16	0.33	0.92
E27	13.32	1.15	8.62	0.14	0.62	1.13
E8	17.61	1.79	10.15	0.13	0.81	0.80

E12	10.26	1.10	10.73	0.16	0.68	0.96
E14	18.16	2.50	13.77	0.13	1.04	0.75
E17	43.34	5.93	13.69	0.12	1.20	0.57
E22	5.19	0.65	12.47	0.12	1.03	0.56
E28	8.41	1.33	15.84	0.11	1.48	0.43
E29	5.90	0.54	9.15	0.14	0.64	0.70

BV/TV = bone volume divided by tissue volume.